CMI

www.nature.com/cmi

ARTICLE

Check for updates

Glycogen synthase kinase 3 controls T-cell exhaustion by regulating NFAT activation

Yubing Fu[1]✉, Jinjia Wang[1], Chenfeng Liu[2], Kunyu Liao[1], Xianjun Gao[1], Ronghan Tang[1], Binbin Fan[1], Yazhen Hong[1], Nengming Xiao[1], Changchun Xiao[3] and Wen-Hsien Liu[1]✉

Cellular immunity mediated by $CD8^+$ T cells plays an indispensable role in bacterial and viral clearance and cancers. However, persistent antigen stimulation of $CD8^+$ T cells leads to an exhausted or dysfunctional cellular state characterized by the loss of effector function and high expression of inhibitory receptors during chronic viral infection and in tumors. Numerous studies have shown that glycogen synthase kinase 3 (GSK3) controls the function and development of immune cells, but whether GSK3 affects $CD8^+$ T cells is not clearly elucidated. Here, we demonstrate that mice with deletion of *Gsk3a* and *Gsk3β* in activated $CD8^+$ T cells (DKO) exhibited decreased CTL differentiation and effector function during acute and chronic viral infection. In addition, DKO mice failed to control tumor growth due to the upregulated expression of inhibitory receptors and augmented T-cell exhaustion in tumor-infiltrating $CD8^+$ T cells. Strikingly, anti-PD-1 immunotherapy substantially restored tumor rejection in DKO mice. Mechanistically, GSK3 regulates T-cell exhaustion by suppressing TCR-induced nuclear import of NFAT, thereby in turn dampening NFAT-mediated exhaustion-related gene expression, including TOX/TOX2 and PD-1. Thus, we uncovered the molecular mechanisms underlying GSK3 regulation of CTL differentiation and T-cell exhaustion in anti-tumor immune responses.

Keywords: GSK3; T-cell exhaustion; Viral infection; Anti-tumor immunity; Inhibitory receptors

Cellular & Molecular Immunology (2023) 20:1127–1139; https://doi.org/10.1038/s41423-023-01075-0

INTRODUCTION

$CD8^+$ T cells are required for the elimination of virus-infected cells and anti-tumor immunity. Antigen-specific naive $CD8^+$ T cells activate, proliferate and differentiate into effector $CD8^+$ T cells and long-lived memory $CD8^+$ T cells during acute infection. Most effector $CD8^+$ T cells die after pathogen clearance in the contraction phase of infection [1]. However, antigen-specific $CD8^+$ cytotoxic lymphocytes (CTLs) exposed to persistent antigen stimulation become exhausted, which is a cellular state characterized by the loss of effector functions and upregulated expression of inhibitory receptors, including PD-1, LAG3, TIM3, and TIGIT. Cells in this state often fail to differentiate into memory $CD8^+$ T cells in the context of chronic viral infection and cancer [2–5]. Immune checkpoint blockade (ICB), such as anti-PD-1 immunotherapy, which can restore T-cell function, has emerged as an effective strategy for the treatment of multiple cancer types in the last decade [6–8]. Although ICB therapy has striking clinical responses, only a minority of cancer patients benefit from ICB therapy due to transient or poor responsiveness to ICB therapy. Therefore, understanding the mechanism(s) underlying ICB therapy non-responsiveness remains a major challenge for the rational design of immunomodulatory strategies [9–11].

Persistent antigen stimulation leads to T-cell exhaustion, which correlates with the severity of dysfunction during chronic infection and cancer. Several transcription factors, NFAT, TOX, c-Myb, BATF, and IRF4, have been shown to control inhibitory receptor expression and T-cell exhaustion [12–16]. NFAT interacts with Fos-Jun (AP-1) to form cooperative NFAT: AP-1 complexes that are critical for the induction of cytokine genes and other activation-associated genes in T cells [17]. However, NFAT is also a crucial regulator of T-cell exhaustion and dysfunction, and NFAT1-binding sites in genes encoding negative regulators and inhibitory receptors have increased chromatin accessibility in dysfunctional and exhausted T cells [12]. Moreover, TCR induces IRF4, BATF, and NFAT expression, and IRF4 and BATF subsequently cooperate with NFAT to upregulate the expression of inhibitory receptors and inhibit memory T-cell development during chronic viral infection [13]. Importantly, TOX is highly expressed in exhausted $CD8^+$ T cells in tumors and chronic viral infection, and TOX expression is induced by TCR-mediated calcium signaling and NFAT activation [18–21]. TOX is necessary and sufficient to induce the major features of exhausted T cells, including the expression of inhibitory receptors, decreased effector T-cell function, and the expression of exhaustion-associated transcription factors [18–22]. Overall, chronic TCR-stimulated NFAT activation leads to NFAT-mediated expression of IRF4, BATF, and TOX, and these transcription factors in turn form a transcriptional circuit to drive the T-cell exhaustion program.

[1]State Key Laboratory of Cellular Stress Biology, School of Life Sciences, Faculty of Medicine and Life Science, Xiamen University, Xiamen 361102 Fujian, China. [2]Department of Cell Biology, School of Life Science, Anhui Medical University, Hefei 230031 Anhui, China. [3]Present address: Sanofi Institute for Biomedical Research, Suzhou, Jiangsu 215123, China. ✉email: fuyubingbio@qq.com; whliu@xmu.edu.cn

Received: 10 March 2023 Accepted: 26 July 2023
Published online: 9 August 2023

Glycogen synthase kinase 3 (GSK3) is a ubiquitous serine/threonine kinase with α and β isoforms, initially described as a key enzyme involved in glycogen metabolism, and has been found to phosphorylate nearly 50 substrates that can strongly affect cell differentiation, proliferation, survival and transformation [23–25]. GSK3 is highly homologous, shows similar substrate specificities, and has been identified as a regulator of many components of the immune system, suggesting that it might be a plausible therapeutic target in inflammatory and autoimmune diseases [26–28]. Interestingly, GSK3β has been identified as an NFAT kinase that phosphorylates conserved serine residues at the N-terminus of NFAT, consequently restraining the nuclear import of NFAT. The expression of constitutionally active GSK3β (GSK-3β S9A) reduces P14 T-cell (TCR specific for LCMV-gp33–41 and H-2D^{b}) proliferation and IL-2 production stimulated with gp33-41 peptide-pulsed macrophages as a result of the sustained nuclear exclusion of NFAT [29]. A previous report demonstrated that GSK3 restores PD-1 expression by suppressing T-bet expression in CTLs and that systemic administration of GSK3 inhibitors promotes CTL function and viral clearance during chronic viral infection [30]. GSK3 inhibitors also enhance anti-tumor immunity by negatively regulating LAG3 expression on CD8$^+$ T cells [31]. However, systemic administration of GSK3 inhibitors also affects other T-cell subsets and immune cells, as well as other tissues. Therefore, the physiological function of GSK3 in CD8$^+$ T cells in the setting of chronic viral infection and cancer is still elusive and needs to be explored and clarified.

In this study, we provided mouse genetic evidence to show that deletion of *Gsk3α* and *Gsk3β* in activated CD8$^+$ T cells resulted in reduced differentiation of effector CD8$^+$ T cells during acute and chronic viral infection and impaired anti-tumor function of CTLs due to increased T-cell exhaustion and expression of inhibitory receptors. Ultimately, our results demonstrate that GSK3 inhibits TCR-mediated nuclear import of NFAT in CD8$^+$ T cells, thereby harnessing the initiation of the T-cell exhaustion program by regulating the NFAT-TOX axis.

RESULTS

GSK3 is required for the differentiation of effector CD8$^+$ T cells during acute and chronic viral infection

To understand the role of GSK3 in effector CD8$^+$ T cells, mice carrying the *loxP*-flanked *Gsk3α* and *Gsk3β* alleles were crossed with *Gzmb* Cre mice expressing Cre recombinase under the control of the granzyme B promoter in activated CD8$^+$ T cells. *Gsk3α*$^{fl/fl}$*Gsk3β*$^{fl/fl}$ (littermate control, WT) and *Gsk3α*$^{fl/fl}$*Gsk3β*$^{fl/fl}$ *Gzmb* Cre (hereafter termed DKO) mice showed normal development of CD8$^+$ T cells in the spleen (Fig. S1A). The percentages, numbers, and activation status of CD8$^+$ T cells in the spleen were largely normal (Fig. S1B). To determine the role of GSK3 in CD8$^+$ T-cell activation, proliferation, and survival, sorted naive CD8$^+$ T cells from WT and DKO mice were activated with anti-CD3 and anti-CD28 antibodies in vitro. The deletion efficiency of *Gsk3α* and *Gsk3β* was completed in DKO CD8$^+$ T cells stimulated with anti-CD3/anti-CD28 antibodies (Fig. S1C). Moreover, we found that GSK3-deficient CD8$^+$ T cells showed normal cell proliferation, apoptosis, and T-cell activation (Fig. S1D–F). WT and DKO mice were then infected with the Armstrong strain of lymphocytic choriomeningitis virus (LCMV-Arm) to establish a murine acute viral infection model. The deletion efficiency of *Gsk3α* and *Gsk3β* in effector CD8$^+$ T cells from DKO mice infected with LCMV-Arm was confirmed by immunoblot analysis (Fig. S1G). The results showed that the expansion of total CD8$^+$ T cells was largely reduced in DKO mice compared with WT mice at the peak of the effector response (Fig. 1A). Upon acute LCMV infection, CD8$^+$ T cells undergo differentiation into short-lived effector cells (SLECs) and memory precursor effector cells (MPECs). We found that the proportion and cell number of SLECs (KLRG1^{hi}CD127^{lo}) in total effector CD8$^+$ T cells were 40% lower in DKO mice than in WT mice, whereas the proportion of MPECs (KLRG1^{lo}CD127^{hi}) was slightly increased in DKO CD8$^+$ T cells (Fig. 1B). Notably, IFNγ and TNFα production by effector CD8$^+$ T cells was markedly reduced in DKO mice compared with their WT counterparts (Fig. 1C). We found that DKO CD8$^+$ T cells exhibited lower expression levels of T-bet and higher expression levels of PD-1, TIM3, and LAG3 than WT CD8$^+$ T cells (Fig. 1D). Unexpectedly, the percentage of progenitor-exhausted PD-1$^+$TIM3$^-$ cells and terminally exhausted PD-1$^+$TIM3$^+$ cells was dramatically increased in DKO CD8$^+$ T cells compared to WT CD8$^+$ T cells (Fig. 1E), suggesting that *Gsk3* deletion in activated CD8$^+$ T cells promotes T-cell exhaustion. These results reveal that GSK3 is essential for the differentiation and function of effector CD8$^+$ T cells during acute viral infection.

To investigate the function of GSK3 in CD8$^+$ T cells upon chronic viral infection, DKO and WT mice were infected with the clone 13 strain of LCMV (LCMV-Cl13) to establish a murine chronic viral infection model. The results showed that expansion of total CD8$^+$ T cells was normal, SLEC differentiation and effector function of CD8$^+$ T cells were reduced, and MPEC generation was increased in DKO mice compared with their WT counterparts at Day 8 after LCMV-Cl13 infection (Fig. S2A, B). Notably, IFNγ, TNFα, and GzmB production by effector CD8$^+$ T cells was markedly reduced in DKO mice compared with their WT counterparts (Fig. S2C, D). Additionally, DKO CD8$^+$ T cells exhibited lower expression levels of T-bet and Bcl2 but higher expression levels of EOMES, TIGIT and PD-1 than WT CD8$^+$ T cells (Fig. S2E). Altogether, these results suggest that GSK3 is essential for the differentiation and function of effector CD8$^+$ T cells and the regulation of T-cell exhaustion during acute and chronic viral infection.

Impaired expansion and differentiation of virus-specific *Gsk3*-deficient CD8$^+$ T cells is cell intrinsic

To directly determine the cell-intrinsic effect of GSK3 on the differentiation of effector CD8$^+$ T cells, we obtained naive CD8$^+$ T cells from DKO P14 (CD45.2$^+$) and WT P14 (CD45.1$^+$CD45.2$^+$) mice, which express a transgene encoding a $V_{\alpha2}{}^+V_{\beta8}{}^+$ TCR specific for gp33-41 of LCMV glycoproteins. DKO and WT P14 cells were then adoptively transferred into WT syngeneic recipient (CD45.1$^+$) mice at a 1:1 ratio followed by LCMV-Arm infection (Fig. 2A). At Days 4.5, 5.5, 6.5, and 7.5 after infection, the expansion of total CD8$^+$ T cells was significantly reduced in DKO P14 cells compared with WT P14 cells (Fig. 2B). In addition, WT effector CD8$^+$ T cells formed a sizable SLEC population, whereas half of DKO effector CD8$^+$ T cells did not differentiate into SLECs but showed increased MPEC differentiation (Fig. 2C), suggesting that GSK3 is crucial for terminal CTL differentiation. Compared with WT P14 cells, production of IFNγ, TNFα and granzyme B by DKO P14 cells was largely decreased at Day 7.5 after LCMV-Arm infection (Fig. 2D). As the transcription Factors T-bet and EOMES control the acquisition of effector function, memory capacity and the exhaustion phenotype of CD8$^+$ T cells [32, 33], we examined T-bet and EOMES expression in P14 cells and found that T-bet expression was diminished, while EOMES and PD-1 expression was upregulated and TIM3 expression was normal in DKO P14 cells relative to their WT counterparts (Fig. 2E, F), suggesting that *Gsk3* deletion results in impaired effector function of CD8+ T cells and an exhausted T-cell phenotype. Since reduced proliferation, increased cell death, or both could lead to the impaired expansion of virus-specific DKO CD8$^+$ T cells, we examined the proliferation and apoptosis of DKO and WT P14 cells. The results showed that cell proliferation of DKO P14 cells assessed by Ki67 expression was not changed, whereas the expression levels of Bcl2 were decreased in DKO P14 cells and the percentage of apoptotic cells determined by intracellular staining of active caspase-3 was slightly elevated in DKO P14 cells relative to WT P14 cells (Fig. 2G–I).

In addition, we generated mixed bone marrow chimeras by reconstituting irradiated *Cd8*$^{-/-}$ mice with bone marrow cells

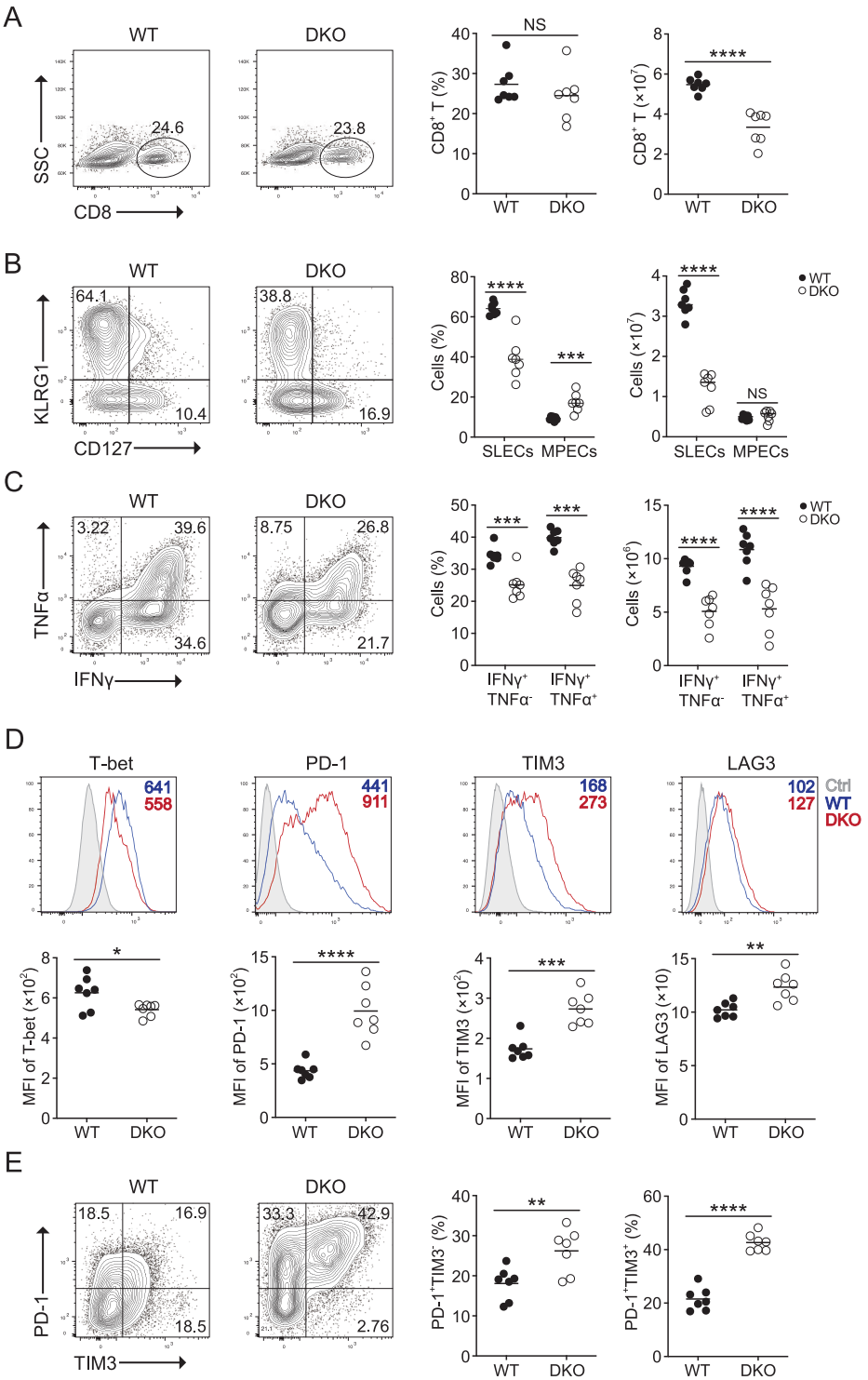

Fig. 1 *Gsk3* deletion alters CD8$^+$ T-cell differentiation during acute viral infection. **A** Flow cytometry analysis of total CD8$^+$ T cells in the spleen from *Gsk3α*$^{fl/fl}$*Gsk3β*$^{fl/fl}$ (WT) and *Gsk3α*$^{fl/fl}$*Gsk3β*$^{fl/fl}$ *Gzmb* Cre (DKO) mice at Day 8 ($n = 7$ per group) after LCMV-Arm infection (left). Summary of the percentage and number of CD8$^+$ T cells (right). **B** Flow cytometry analysis of SLECs (KLRG1^{hi}CD127^{lo}) and MPECs (KLRG1^{lo}CD127^{hi}) gated on CD8$^+$CD44$^+$ T cells from (**A**) (left). Summary of the percentage and cell number of SLECs and MPECs (right). **C** Flow cytometry analysis of IFNγ and TNFα production gated on CD8$^+$CD44$^+$ T cells from (**A**) (left). Summary of the percentage and cell number of IFNγ$^+$TNFα$^+$ and IFNγ$^+$TNFα$^-$ cells (right). **D** Flow cytometry analysis of T-bet, PD-1, TIM3, and LAG3 expression among CD8$^+$CD44$^+$ T cells (upper). Summary of MFI (mean fluorescence intensity) (lower). **E** Flow cytometry analysis of PD-1 and TIM3 gated on CD8$^+$CD44$^+$ T cells from (**A**) (left). Summary of the percentage of PD-1$^+$TIM3$^-$ and PD-1$^+$TIM3$^+$ cells (right). Each symbol represents an individual mouse. Small horizontal lines indicate the mean (±SD). *$P < 0.5$; **$P < 0.01$; ***$P < 0.001$; ****$P < 0.0001$. NS not significant. Data are representative of three independent experiments

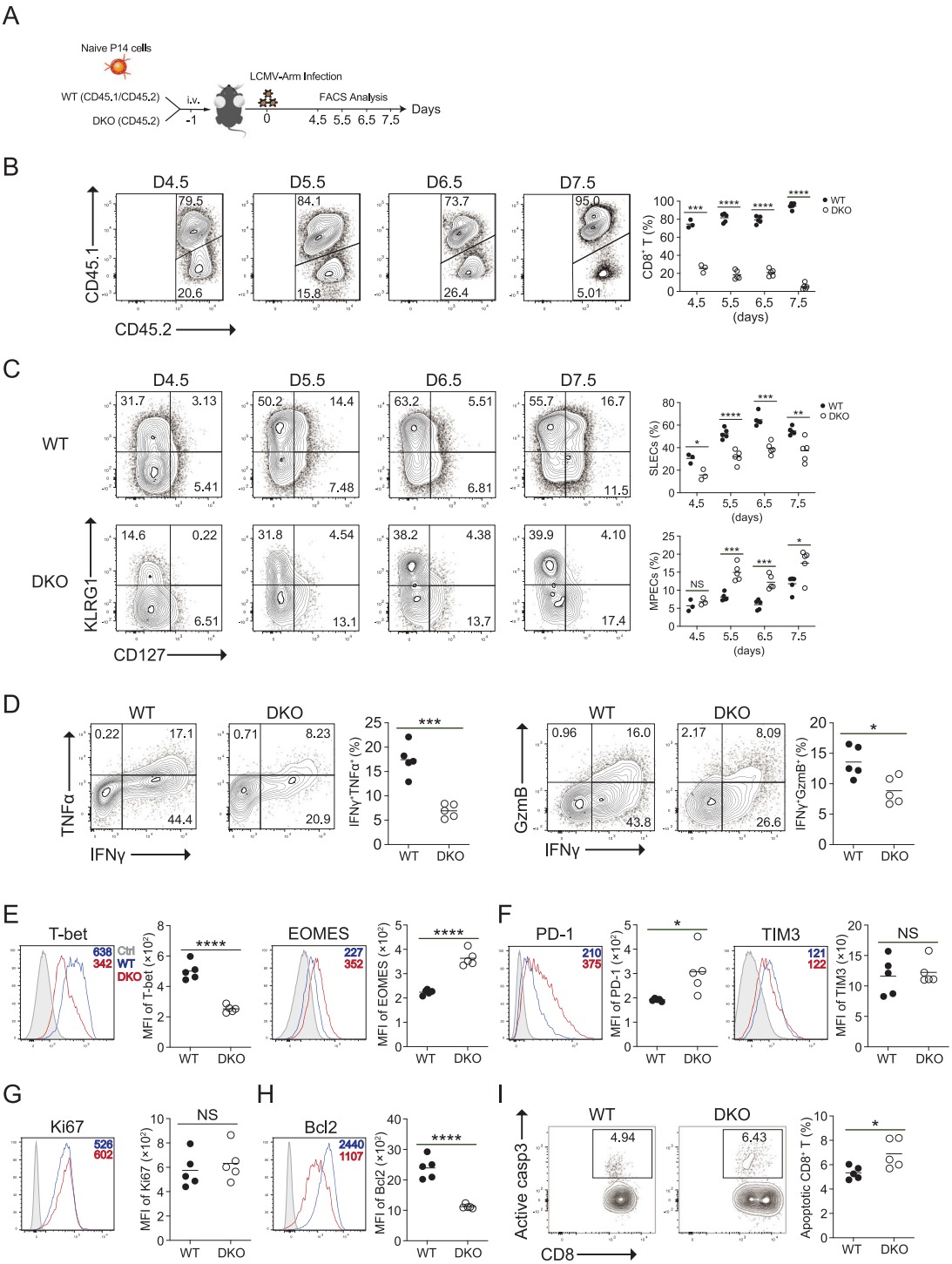

Fig. 2 GSK3 regulates antigen-specific effector CD8$^+$ T-cell differentiation during acute viral infection. **A** A total of 5×10^4 sorted *Gsk3α*$^{fl/fl}$*Gsk3β*$^{fl/fl}$ P14 (WT, CD45.1/CD45.2) and *Gsk3α*$^{fl/fl}$*Gsk3β*$^{fl/fl}$ P14 *Gzmb* Cre (DKO, CD45.2) CD8$^+$ T cells were mixed at a ratio of 1:1 and cotransferred into WT CD45.1 hosts, followed by LCMV-Arm infection 24 h after cell transfer. **B** Flow cytometry analysis of WT and DKO P14 cells in the spleen from the recipients on Days 4.5 ($n = 3$ per group), 5.5 ($n = 5$ per group), 6.5 ($n = 5$ per group) and 7.5 ($n = 5$ per group) after LCMV-Arm infection (left). Summary of the percentage of CD8$^+$ T cells (right). **C** Flow cytometry analysis of SLECs (KLRG1^{hi}CD127^{lo}) and MPECs (KLRG1^{lo}CD127^{hi}) gated on CD8$^+$CD44$^+$ T cells from (**B**) (left). Summary of the percentage of SLECs (KLRG1^{hi}CD127^{lo}) and MPECs (KLRG1^{lo}CD127^{hi}) (right). **D** Flow cytometry analysis of IFNγ, TNFα, and granzyme B (GzmB) production by CD8$^+$CD44$^+$ T cells on Day 7.5 after LCMV-Arm infection (left). Summary of the percentage of IFNγ$^+$TNFα$^+$ and IFNγ$^+$GzmB$^+$ cells (right). **E–H** Flow cytometry analysis of T-bet and EOMES (**E**), PD-1 and TIM3 (**F**), Ki67 (**G**), and Bcl2 (**H**) gated on CD8$^+$CD44$^+$ T cells on Day 7.5 after LCMV-Arm infection (left). Summary of MFI (right). **I** Flow cytometry analysis of activated caspase-3 (Active casp3) in CD8$^+$CD44$^+$ T cells on Day 7.5 after LCMV-Arm infection (left). Summary of the percentage of CD8$^+$ active casp3$^+$ cells (right). Each symbol represents an individual mouse. Small horizontal lines indicate the mean (±SD). *$P < 0.5$; **$P < 0.01$; ***$P < 0.001$; ****$P < 0.0001$. NS not significant. Data are representative of three independent experiments

from DKO (CD45.2$^+$) or WT (CD45.2$^+$) plus WT (CD45.1$^+$) congenic donors (Fig. S3A). Two months after bone marrow reconstitution, these chimeric mice were infected with LCMV-Arm. The results showed that the expansion of DKO CD45.2$^+$CD8$^+$ T cells was reduced compared with that of their WT counterparts on Day 8 after LCMV-Arm infection (Fig. S3B). In addition, we found that the proportion and cell number of SLECs were 60–70% lower in DKO CD8$^+$ T cells than in WT CD8$^+$ T cells, whereas the frequency of MPECs was increased but the MPEC cell number was normal in DKO CD8$^+$ T cells (Fig. S3C). Compared with that of WT CD8$^+$ T cells, the production of IFNγ and granzyme B by DKO P14 cells was largely decreased on Day 8 after LCMV-Arm infection (Fig. S3D). Moreover, DKO CD8$^+$ T cells exhibited lower expression levels of T-bet and higher expression levels of PD-1, TIGIT, TOX/TOX2, and EOMES than their WT counterparts (Fig. S3E). Altogether, these results reveal that GSK3 regulates the expansion and differentiation of effector CD8$^+$ T cells in a cell-intrinsic manner.

GSK3 is required for CD8$^+$ T-cell-mediated anti-tumor immune responses

Persistent antigen stimulation of CD8$^+$ T cells in tumors promotes the generation of exhausted T cells, which display impaired cytokine production and upregulation of inhibitory receptors. We thus wondered whether GSK3 regulates CTL function and T-cell exhaustion in anti-tumor T-cell immune responses. To this end, we subcutaneously (s.c.) implanted B16-F10 melanoma, MC38, or LLC-1 cells into DKO mice and WT littermates and monitored tumor growth. The results showed that DKO mice displayed a greater tumor burden than WT mice in these three tumor models (Fig. 3A–C). Accordingly, IFNγ and TNFα production by CD8$^+$ T cells in tumor-infiltrating lymphocytes (TILs) was drastically reduced in B16-F10-inoculated DKO mice compared to their WT counterparts (Fig. 3D). In addition, we found that the percentage of terminally exhausted PD-1$^+$TIM3$^+$ cells in DKO CD8$^+$ TILs was significantly higher than that in WT CD8$^+$ TILs, whereas the percentage of progenitor-exhausted PD-1$^+$TIM3$^-$ cells was not changed in DKO CD8$^+$ TILs (Fig. 3E), indicating that GSK3 prevents the formation of terminally exhausted CD8$^+$ T cells in tumors. Moreover, compared with their WT counterparts, GSK3-deficient CD8$^+$ TILs also exhibited markedly decreased production of granzyme B and perforin (Fig. 3F). Altogether, our results reveal that GSK3 is indispensable for the effector function of CD8$^+$ T cells and the regulation of T-cell exhaustion in anti-tumor immune responses.

Deletion of *Gsk3* limits the effector function of tumor-specific CD8$^+$ T cells

We next assessed tumor-specific T-cell responses in mice implanted with B16-F10 cells expressing LCMV glycoprotein gp33-41 (B16-gp33) followed by adoptive transfer of in vitro activated DKO or WT P14 CTLs (Fig. 4A). The results showed that B16-gp33 tumor-bearing mice receiving DKO P14 CTLs exhibited increased tumor growth and poor survival compared to mice receiving WT P14 CTLs (Fig. 4B, C). As PD-1 blockade immunotherapy greatly improved anti-tumor T-cell responses, we wondered whether the dysfunction of GSK3-deficient CD8$^+$ TILs is due to increased PD-1 expression levels. To test this hypothesis, B16-gp33-harboring mice were transferred with DKO or WT P14 CTLs and then administered anti-PD-1 antibodies. Strikingly, treatment with anti-PD-1 greatly diminished the tumor burden and enhanced the survival of mice transferred with DKO P14 cells compared with the isotype control DKO group mice, which were similar to WT P14 CTL-transferred mice (Fig. 4D, E).

Furthermore, we employed a B16-F10 lung metastasis model with P14 cell transfer (Fig. 4F). The results showed that the number and size of metastatic foci in the lung were drastically increased in B16-gp33-implanted mice receiving DKO P14 CTLs compared to their WT counterparts (Fig. 4G). T-bet and Ki67 expression was downregulated in DKO P14 cells relative to their WT counterparts (Fig. 4H). In addition, the numbers of progenitor-exhausted PD-1$^+$TIM3$^-$ cells and terminally exhausted PD-1$^+$TIM3$^+$ cells in DKO P14 TILs were significantly higher than those in WT P14 TILs (Fig. 4I), indicating that GSK3 prevents the formation of progenitor and terminally exhausted antigen-specific CD8$^+$ T cells in metastatic tumors. Importantly, PD-1 blockade treatment fully restored antitumor T-cell immunity in B16-F10 lung metastases in DKO P14 cell-transferred mice (Fig. 4J). These results indicate that GSK3 is crucial for anti-tumor T-cell immunity in metastatic cancer.

To examine whether GSK3 affects CTL function, we performed an in vitro killing assay by using DKO or WT P14 CTLs incubated with EL4-gp33 cells as target cells. As shown in Fig. S4, DKO P14 CTLs displayed decreased cytolysis of EL4-gp33 cells compared with WT P14 CTLs, suggesting that *Gsk3* deletion in CD8$^+$ T cells reduced CTL function. Altogether, our findings suggest that GSK3 promotes CD8$^+$ T-cell-mediated anti-tumor immune responses by restraining T-cell exhaustion and regulating PD-1 expression.

Transcriptional signatures reveal that GSK3 regulates TOX/TOX2 expression in CD8$^+$ T cells

To gain insights into the molecular mechanisms underlying GSK3 regulation of CD8$^+$ T-cell function and exhaustion, we performed transcriptome analysis of transferred DKO and WT CD44$^+$ P14 cells from recipient mice infected with LCMV-Arm at day 5.5 by RNA sequencing (RNA-seq) analysis. The results of gene set enrichment analysis (GSEA) showed that genes encoding molecules related to the IL-2/STAT5 signaling pathway, IFNγ response, TNFα/NFκB signaling pathway, and inflammatory response were enriched in DKO P14 cells (Fig. 5A, Fig. S5), which was correlated with decreased effector function and differentiation of CD8$^+$ T cells in DKO P14 cells during acute viral infection. Moreover, detailed analysis of RNA-seq data indicated a significant difference in gene expression between DKO and WT P14 cells; a total of 3084 genes displayed a difference in expression of more than twofold. *Tox*, *Tox2*, *Myb*, Eomes, and *Tigit* mRNAs were upregulated, and *Tbx21*, *Klrg1*, *Bach2*, and *Bcl2* mRNAs were downregulated in DKO P14 cells compared with WT P14 cells (Fig. 5B). Among these genes, transcription factor and inhibitory receptor genes downregulated or upregulated in DKO P14 cells are known to regulate immune-associated function and T-cell exhaustion (Fig. 5C). Interestingly, the TOX/TOX2 family has been shown to induce T-cell exhaustion in different mouse tumor and chronic viral infection models as well as in cancer patients and to facilitate endocytic recycling of PD-1 [18, 19, 34]. We found that the expression of Tox and *Tox2* mRNA was upregulated by *Gsk3* deletion, suggesting that GSK3 regulates TOX/TOX2 expression at the transcriptional level. Next, we compared TOX/TOX2 expression in DKO and WT CD8$^+$ T cells by flow cytometry. The results demonstrated that TOX/TOX2 expression was markedly upregulated in transferred DKO P14 cells from recipients infected with LCMV-Arm relative to the WT P14 group and CD8$^+$ TILs in DKO mice with B16 lung metastasis compared with their WT counterparts (Fig. 5D, E), indicating that GSK3 regulates TOX/TOX2 expression in CD8$^+$ T cells. Altogether, these results reveal that GSK3 regulates the expression of TOX/TOX2, other transcription factors related to effector function and differentiation of CD8$^+$ T cells, and inhibitory receptors involved in T-cell exhaustion.

GSK3 regulates TCR-mediated NFAT activation in activated CD8$^+$ T cells

NFAT is a crucial regulator of T-cell exhaustion, and NFAT-binding sites in genes encoding negative regulators and inhibitory receptors have increased chromatin accessibility in exhausted T cells [12]. TCR-mediated NFAT activation has been shown to regulate TOX expression [18–21], and constitutively active GSK3β promotes cytosolic retention of NFAT in CD8$^+$ T cells [29]. Thus, we wondered whether GSK3 controls T-cell exhaustion and TOX

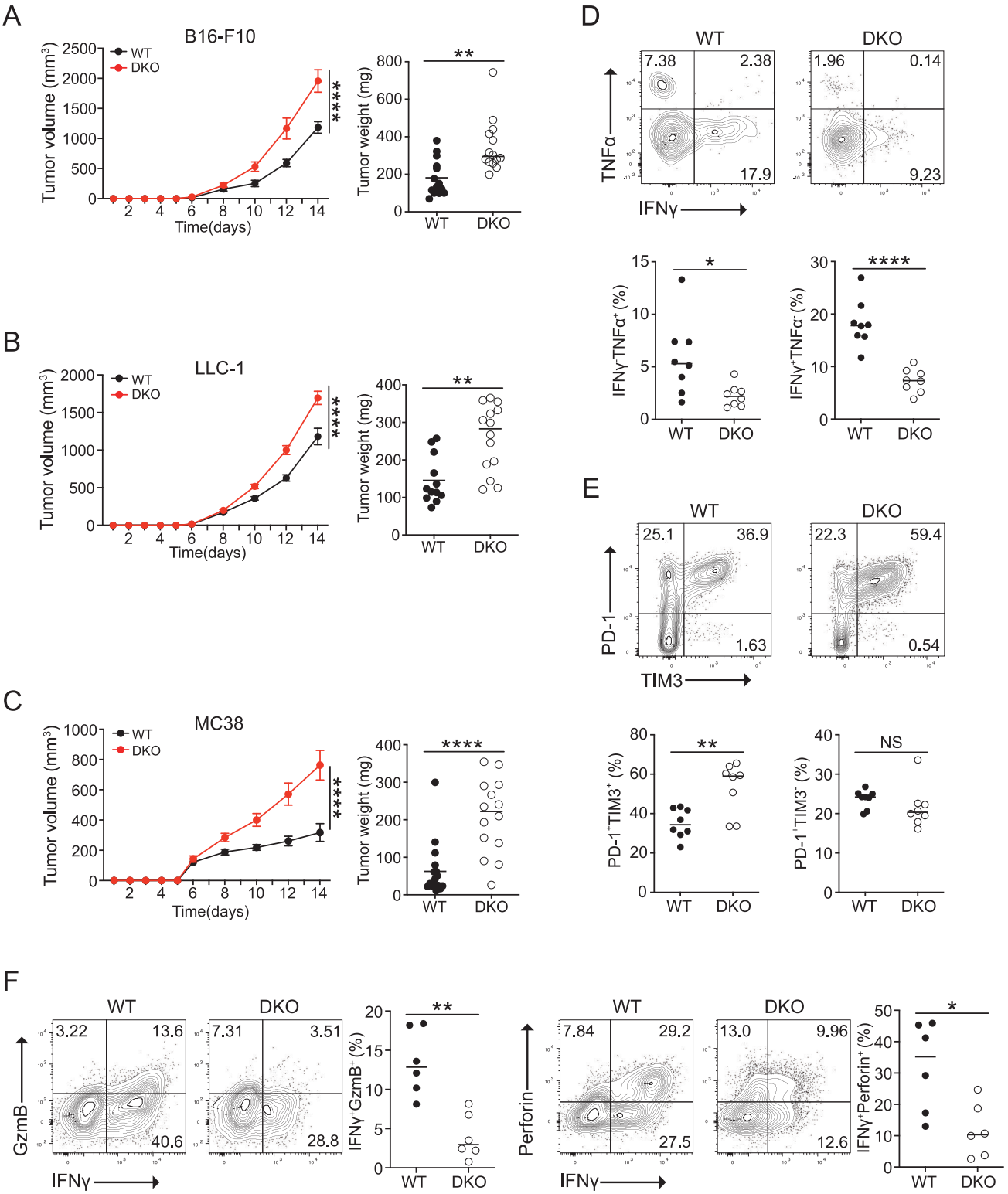

Fig. 3 Deletion of *Gsk3* leads to reduced CTL function in tumors. **A**–**C** Tumor volume of DKO and WT mice ($n = 7$) inoculated with 1×10^6 B16-F10 (**A**), MC38 (**B**), or LLC-1 (**C**) cells by subcutaneous injection into two flanks. Tumor growth was determined by measurement of tumor size (left), and the tumor weight of solid tumors isolated from DKO and WT mice was measured at the experimental endpoint (right). **D** Flow cytometry analysis of IFNγ and TNFα production by tumor-infiltrating $CD8^+$ T cells in (**A**) (upper). Summary of the percentage of $IFN\gamma^-TNF\alpha^+$ and $IFN\gamma^+TNF\alpha^-$ cells (lower). **E** Flow cytometry analysis of PD-1 and TIM3 expression in (**A**) (upper). Summary of the percentage of $PD\text{-}1^+TIM3^+$ and $PD\text{-}1^+TIM3^-$ cells (lower). **F** Flow cytometry analysis of IFNγ, GzmB, and perforin production by tumor-infiltrating $CD8^+$ T cells from (**C**) (left). Summary of the percentage of $IFN\gamma^+GzmB^+$ and $IFN\gamma^+Perforin^+$ cells (right). Small horizontal lines indicate the mean (±SD) tumor volume statistics (±SEM). $^*P < 0.5$; $^{**}P < 0.01$; $^{****}P < 0.0001$. NS not significant. Data are representative of three independent experiments

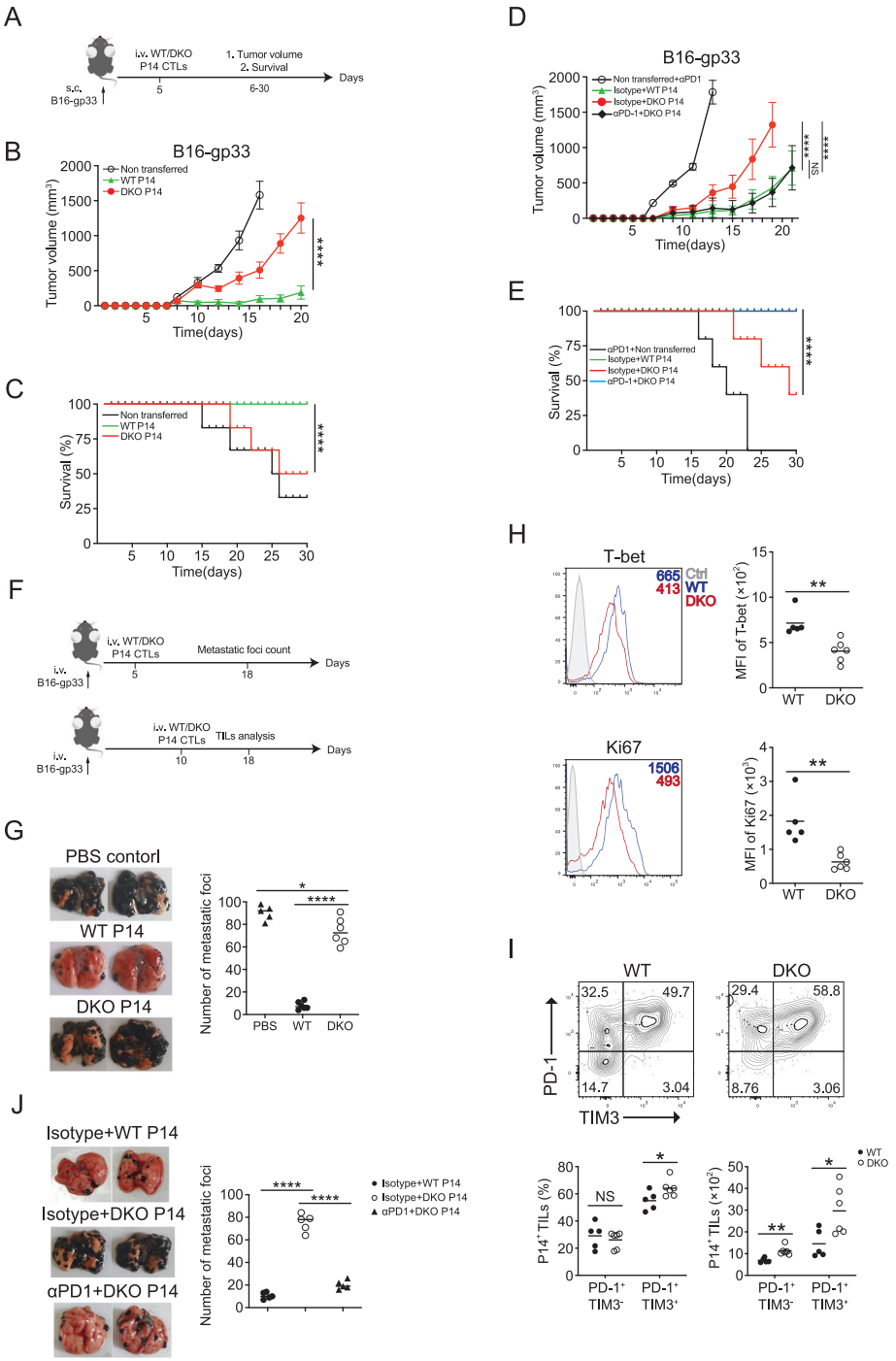

Fig. 4 GSK3 is necessary for the antitumor function of tumor-specific CD8$^+$ T cells. **A** Experimental outline of P14 transfer in a B16-gp33 melanoma model. B6 (CD45.1) mice were inoculated with 1×10^6 B16-gp33 melanoma cells by subcutaneous injection into the middle of the back, followed by adoptive transfer of 1×10^6 activated DKO or WT P14 cells on Day 5 ($n = 6$ per group). **B**, **C** Tumor volume (**B**) and the survival rate of mice (**C**) in (**A**). **D**, **E** *Cd8*$^{-/-}$ mice were inoculated with 1×10^6 B16-gp33 melanoma cells by subcutaneous injection into the middle of the back, followed by adoptive transfer of 1×10^6 activated DKO or WT P14 cells on Day 5 ($n = 5$ per group). Mice were treated with either isotype control antibodies or anti-PD-1 blocking antibodies on Days 6, 9, and 12. Tumor volume (**D**) and the survival rate of mice (**E**) are shown. (**F**) Experimental outline of the B16-gp33 lung metastasis model. Representative photograph of pulmonary metastatic foci in recipient mice ($n \geq 5$ per group) receiving B16-gp33 cells via tail vein injection and then treated with PBS or transferred with WT P14 or DKO P14 cells on Day 5 (**G**) or Day 10 (**H**, **I**). (**G**) Representative photograph of pulmonary metastatic foci (left). Numbers of metastatic foci in the lungs from the indicated groups (right). **H** Flow cytometry analysis of T-bet and Ki67 gated on CD8$^+$CD44$^+$ T cells from TILs in the lung from the indicated group (left). Summary of MFI (right). **I** Flow cytometry analysis of PD-1 and TIM3 expression gated on CD8$^+$CD44$^+$ T cells from TILs in the lung from the indicated group (upper). Summary of the percentage of PD-1$^+$TIM3$^+$ and PD-1$^+$TIM3$^-$ cells (lower). **J** Representative photograph of pulmonary metastatic foci (upper). Numbers of metastatic foci in the lungs from the indicated groups (lower). Small horizontal lines indicate the mean (±SD). Statistics in tumor volume (±SEM). *$P < 0.5$; **$P < 0.01$; ***$P < 0.001$; ****$P < 0.0001$. NS not significant. Data are representative of three independent experiments

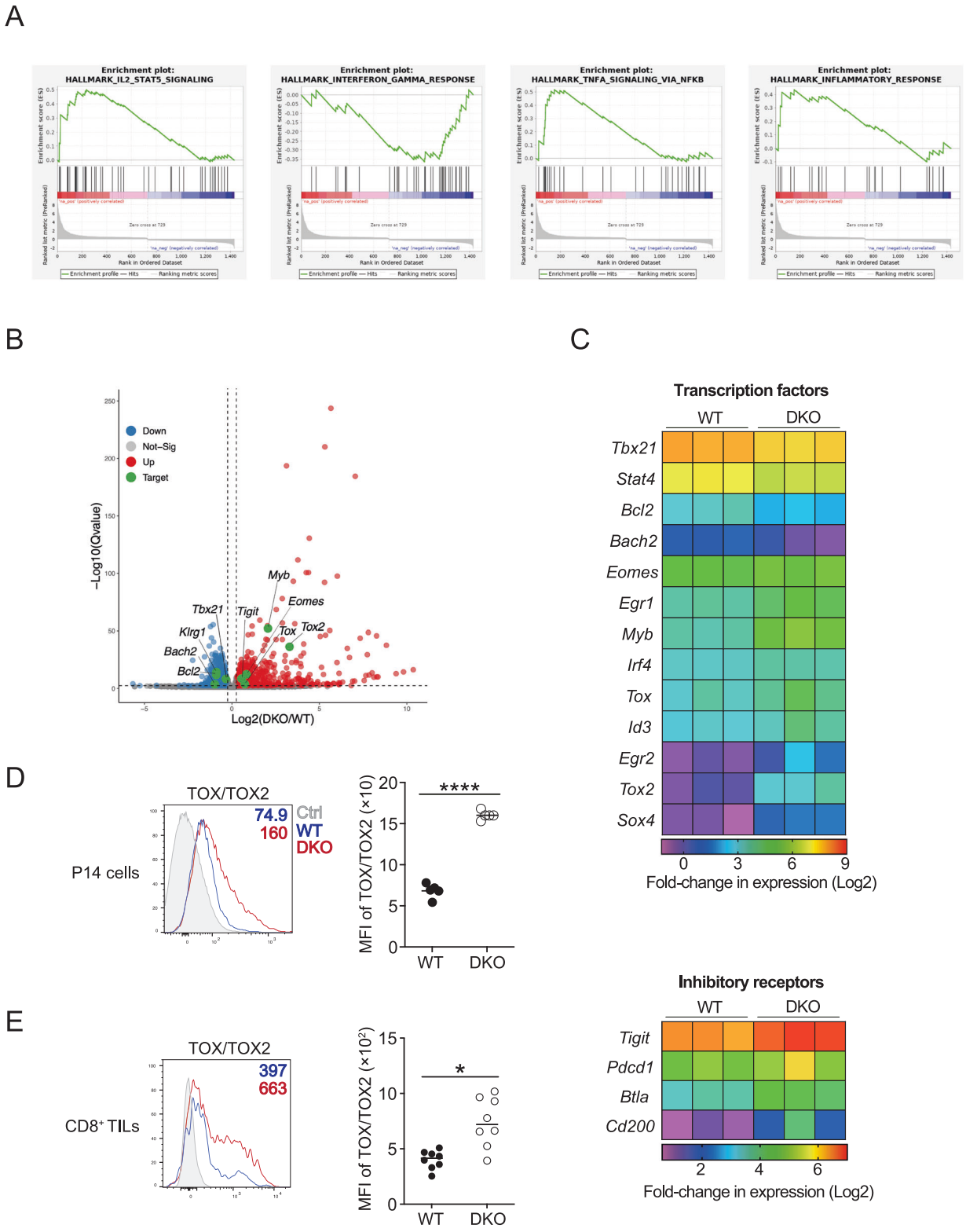

Fig. 5 TOX/TOX2 expression is regulated by GSK3 in CD8$^+$ T cells. WT CD45.1 mice were transferred with 5×10^4 DKO P14 or WT P14 cells, followed by LCMV-Arm infection 24 h after cell transfer. RNA samples from DKO P14 or WT P14 cells in recipients on Day 5.5 after LCMV-Arm infection were prepared for RNA-seq analysis. **A** Gene set enrichment analysis (GSEA) using hallmark gene sets showed that IL-2/STAT5 signaling, IFNγ response, TNFα signaling via NFκB, and inflammatory response were altered in DKO P14 cells. **B** Volcano plots of genes differentially expressed in WT and DKO P14 cells. **C** Differentially expressed genes (DEGs) between WT and DKO CD8$^+$ T cells were grouped into transcription factors (upper) and inhibitory receptors (lower). **D** Flow cytometry analysis of TOX/TOX2 expression gated on CD8$^+$CD44$^+$ T cells among WT and DKO P14 cells (left). Summary of MFI of TOX/TOX2 (right). **E** Flow cytometry analysis of TOX/TOX2 gated on CD8$^+$CD44$^+$ TILs in the lung from Fig. 4G (left). Summary of MFI of TOX/TOX2 (right). Each symbol represents an individual mouse. Small horizontal lines indicate the mean (±SD). *$P < 0.5$; ****$P < 0.0001$. Data are representative of two independent experiments

expression by regulating NFAT activation. To test this hypothesis, we first tested whether *Gsk3* deletion affects the nuclear localization of NFAT in activated $CD8^+$ T cells. Transferred DKO and WT P14 cells from the recipients infected with LCMV-Arm were sorted for immunoblot and confocal imaging analysis. The results showed that *Gsk3* deficiency promoted the nuclear translocation of NFAT1 and NFAT2 in activated $CD8^+$ T cells (Fig. 6A, B). Moreover, the levels of nuclear-localized NFAT1 and NFAT2 were largely increased in activated DKO $CD8^+$ T cells restimulated with anti-CD3 and anti-CD28 antibodies or PMA plus ionomycin compared with activated WT $CD8^+$ T cells (Fig. 6C, D). These results reveal that GSK3 regulates TCR/CD28-induced NFAT activation by promoting the nuclear export of NFAT in activated $CD8^+$ T cells.

GSK3 controls the anti-tumor function of $CD8^+$ T cells by regulating the NFAT-TOX axis

To demonstrate that GSK3-mediated NFAT activation is involved in T-cell exhaustion in anti-tumor T-cell immunity, DKO $Cas9^{tg/+}$ P14 cells were transduced with retroviruses encoding small guide RNAs (sgRNAs) targeting *Nfatc1, Nfatc2* or nontarget control (NTC). sgRNA-transduced P14 cells were then transferred into B16-gp33 implanted $Cd8^{-/-}$ recipients, and tumor growth was measured (Fig. 7A). Notably, we found that mice receiving *Nfatc1* or *Nfatc2* sgRNA-transduced DKO P14 cells showed more significant tumor regression than mice receiving NTC sgRNA-transduced DKO P14 cells (Fig. 7B), indicating that *Nfatc1* or *Nfatc2* deletion in DKO P14 cells restored $CD8^+$ T-cell function in anti-tumor immunity. To determine whether TOX and TOX2 contribute to the GSK3-mediated regulation of $CD8^+$ T cell anti-tumor function, sorted $CD8^+$ T cells from WT and DKO $Cas9^{tg/+}$ P14 mice were transduced with retroviruses encoding sgRNAs targeting *Tox*, *Tox2* or NTC sgRNAs. B16-gp33-bearing $Cd8^{-/-}$ mice were then transferred with sgRNA-transduced P14 cells. As shown in Fig. 7C, D, mice receiving *Tox* or *Tox2* sgRNA-transduced DKO P14 cells showed greater tumor regression than the NTC DKO P14 group, which was similar to *Pdcd1* deletion in the DKO P14 group, suggesting that either *Tox* or *Tox2* deletion in DKO P14 cells restored anti-tumor T-cell function.

We next tested whether *Nfatc2, Tox*, and *Tox2* deletion rescued the exhausted phenotype in DKO P14 cells by analyzing TOX/TOX2, T-bet, and PD-1 expression. To this end, $Cd8^{-/-}$ mice were intravenously injected with B16-gp33 cells, followed by adoptive transfer of WT P14 cells transduced with NTC sgRNA retroviruses or DKO P14 cells transduced with *Nfatc2, Tox, Tox2* or NTC sgRNA retroviruses. At 10 days after P14 cell transfer, TILs in the lungs from the recipients were isolated and analyzed by flow cytometry. The results showed that reduced expression levels of TOX/TOX2 were observed in *Tox*- or *Tox2* sgRNA-positive (GFP^+BFP^+) DKO $Cas9^{tg/+}$ P14 cells compared with NTC sgRNA-transduced DKO $Cas9^{tg/+}$ P14 cells (Fig. 7E). Importantly, *Nfatc2, Tox* and *Tox2* deletion substantially restored T-bet and PD-1 expression in DKO P14 cells in TILs (Fig. 7F, G). Altogether, these results demonstrate that GSK3 controls $CD8^+$ T-cell function in tumors by regulating NFAT-mediated TOX/TOX2 and PD-1 expression (Fig. 8).

DISCUSSION

GSK3 phosphorylates multiple target proteins to regulate various biological processes. Among these pathways, Wnt/β-catenin signaling is well known and tightly regulated by GSK3 through GSK3-mediated β-catenin phosphorylation and subsequent degradation through the ubiquitination-proteasome pathway [35]. Our previous study demonstrated that in the absence of GSK3, β-catenin accumulated in the cytoplasm, where it associated with and activated Akt, leading to the phosphorylation and degradation of Foxo1 and the downregulation of Klf2 and $S1P_1$ expression, thereby preventing the emigration of thymocytes [36]. However, we found that *Ctnnb1* deletion in *Gsk3*-deficient $CD8^+$ T cells failed to restore the differentiation and function of $CD8^+$ T cells (data not shown), suggesting that β-catenin does not contribute to the GSK3-mediated regulation of $CD8^+$ T cell differentiation and function. Thus, GSK3 may regulate T-cell differentiation and function in a cell context-dependent manner. In this study, we demonstrated that GSK3 regulates the differentiation of effector $CD8^+$ T cells and T-cell exhaustion. Importantly, we identified that GSK3 prevents TCR-stimulated NFAT nuclear import to control NFAT-mediated activation of the T-cell exhaustion transcriptional program, including TOX/TOX2 and PD-1 expression.

GSK3 siRNAs or inhibitors have been shown to downregulate PD-1 expression by upregulating CTL T-bet expression, which in turn promotes CTL function and viral clearance during chronic viral infection [30]. Moreover, the same group demonstrated that GSK3 inhibitors enhance anti-tumor immunity by negatively regulating LAG3 expression on $CD8^+$ T cells [31]. However, our results clearly showed that mice with *Gsk3α* and *Gsk3β* deletion in activated $CD8^+$ T cells resulted in reduced differentiation of effector $CD8^+$ T cells and T-bet expression during acute and chronic viral infection and compromised anti-tumor T-cell function due to increased nuclear NFAT localization, thereby upregulating the expression of TOX/TOX2 and PD-1 and promoting the T-cell exhaustion program. Treatment with GSK3 inhibitors enhances NFAT activation to promote the activation of naive $CD8^+$ T cells, but it may conversely promote T-cell exhaustion in activated $CD8^+$ T cells due to the sustained nuclear import of NFAT. To bypass the effects of GSK3 on T-cell activation, mice with *Gsk3α* and *Gsk3β* deletion specifically in activated $CD8^+$ T cells were used to study the physiological function of GSK3 in effector $CD8^+$ T-cell differentiation and T-cell exhaustion. Interestingly, our unpublished data demonstrated that GSK3 inhibitors significantly suppressed PD-1 expression in both WT and DKO $CD8^+$ T cells, suggesting that GSK3 inhibitors target not only GSK3 but also other unknown pathways to downregulate PD-1 expression. Notably, systemic administration of GSK3 inhibitors or siRNAs targets not only $CD8^+$ T cells but also other immune cells and tissues and may have off-target effects in cells. Intriguingly, our preliminary data showed that Gsk3α and Gsk3β deletion in regulatory T (Treg) cells impaired Treg cell function, thereby promoting Th1 cell differentiation and $CD8^+$ T-cell activation (data not shown), suggesting that treatment with GSK3 inhibitors not only promotes CTL function but also leads to reduced Treg cell function, which in turn augments $CD8^+$ T-cell activation. Thus, the application of GSK3 inhibitors or siRNAs in cancer therapy warrants further evaluation and investigation.

GSK3 regulates the phosphorylation of NFAT to control T-cell activation and exhaustion. During early acute infection, following activation of naive T cells, calcium influx from TCR ligation results in the nuclear localization of NFAT, where these transcription factors form heterodimers with AP-1 family members to promote the transactivation of functional Teff effector genes [12, 37]. During late acute infection, the elimination of the virus induces the attenuation of the effector and activation in $CD8^+$ T cells. However, in *Gsk3*-deficient $CD8^+$ T cells, the balance of NFAT and AP-1 favors high NFAT levels and low AP-1 levels, perhaps due to BATF antagonizing the formation of canonical Fos/Jun AP-1 complexes, triggering partnerless NFAT nuclear accumulation independent of AP-1 [38–41]. This partnerless NFAT binds to the locus of exhaustion-related genes, including *Tox/Tox2* and *Pdcd1*, to induce their expression, and TOX/TOX2 subsequently induces the expression of PD-1 and other inhibitory receptors. Our findings demonstrate that GSK3 inhibits the nuclear translocation of NFAT in activated $CD8^+$ T cells, thereby restraining the NFAT-TOX-mediated T-cell exhaustion program during acute and chronic viral infection and cancer.

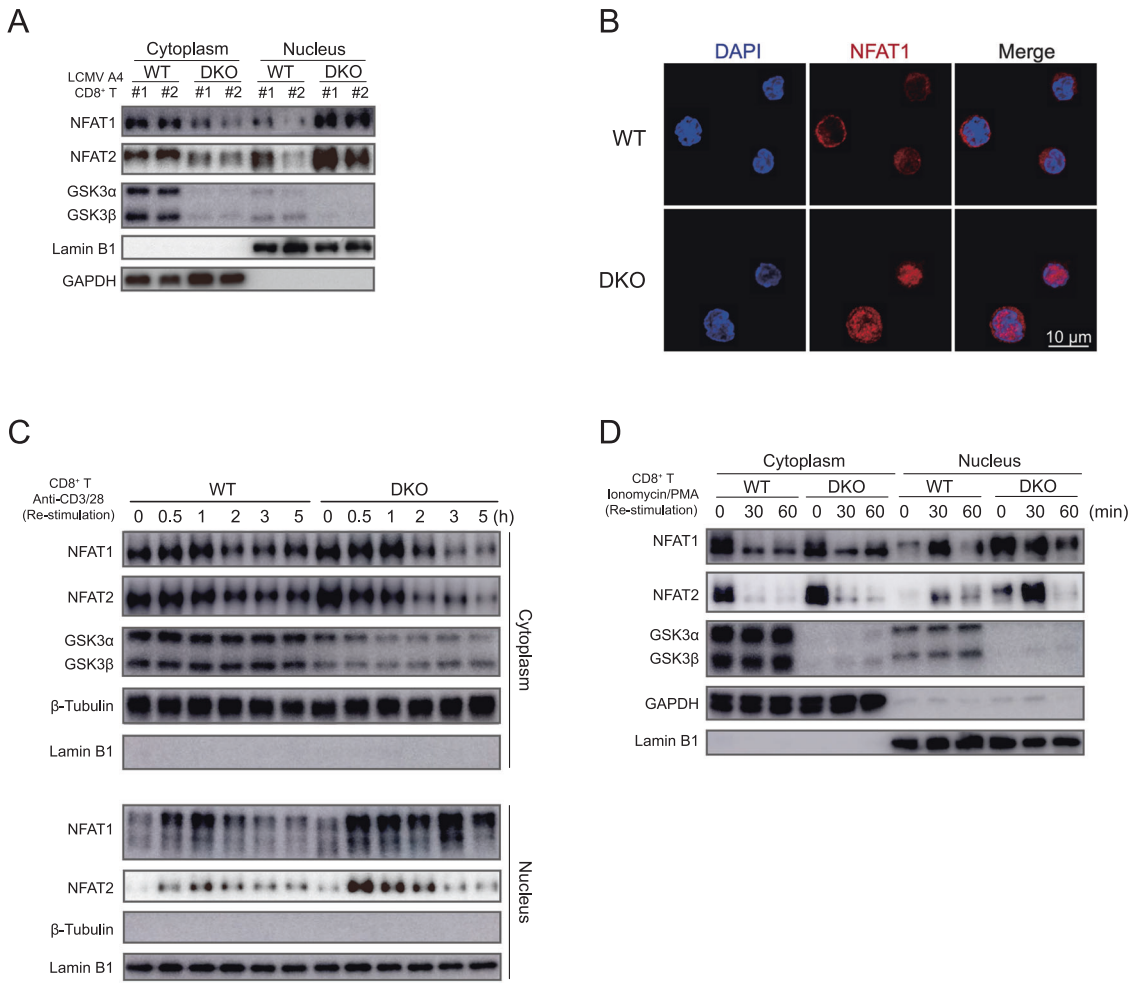

Fig. 6 *Gsk3* deletion promotes the nuclear import of NFAT in $CD8^+$ T cells. **A** B 1×10^5 WT or DKO P14 (CD45.2) cells were transferred into WT CD45.1 hosts, followed by LCMV-Arm infection. DKO and WT P14 cells were sorted 7.5 days after LCMV-Arm infection. Immunoblot analysis of NFAT1, NFAT2, GSK3α/β, GAPDH, and Lamin B1 in cytoplasmic and nuclear fractions of WT and DKO P14 cells (**A**). Representative immunofluorescence images of WT and DKO P14 cells stained for NFAT1 (red) and 4′,6-diamidino-2-phenylindole (DAPI; blue, nuclear staining) (**B**). Scale bars, 10 μm. **C**, **D** Immunoblot analysis of NFAT1, NFAT2, GSK3α/β, GAPDH, β-tubulin, and lamin B1 in cytoplasmic and nuclear fractions of activated WT and DKO $CD8^+$ T cells restimulated with anti-CD3/anti-CD28 (**C**) or ionomycin/PMA (**D**) for the indicated amounts of time. Data are representative of two independent experiments

MATERIALS AND METHODS

Mice

Gsk3α$^{fl/fl}$, *Gsk3β*$^{fl/fl}$, *Gzmb* Cre (Jax stock 003734), P14 (Jax stock 037394), CD8KO (Jax stock 002665), B6 CD45.1$^+$ (Jax stock 002014), and Rosa26$^{LSL\text{-}Cas9}$ (Jax stock 028551) mice were previously reported [36]. Unless otherwise noted, *Gsk3α*$^{fl/fl}$*Gsk3β*$^{fl/fl}$ *Gzmb* Cre mice were analyzed at 8 to 12 weeks of age, while other mice were used as donors or recipients at 8 to 12 weeks of age. All mice were bred and housed under specific pathogen-free conditions. All animal experiments were approved by the Animal Care and Use Committee of Xiamen University.

Adoptive transfer and LCMV infection

For the adoptive transfer experiments, 1×10^5 naive P14 cells were purified by fluorescence-activated cell sorting and adoptively transferred into host mice 1 day before LCMV-Arm or LCMV-Cl13 infection. For acute and chronic viral infection, mice were intravenously injected with 2×10^5 plaque-forming units LCMV-Arm and 2×10^6 plaque-forming units LCMV-Cl13, respectively.

Cell culture and cellular assays

$CD8^+$ T cells were cultured in RPMI medium (Gibco) supplemented with 10% FBS (EXCELL Biotech), 25 mM HEPES (Sigma), 100 units/mL penicillin-G, 100 μg/mL streptomycin (Gibco), and 50 μM β-ME. For adoptive cell transfer, total splenocytes isolated from WT and DKO P14 cells were activated with gp33 peptides (2 ng/mL) in the presence of IL-2 (20 ng/mL). Five days later, total $CD8^+$ T cells (1×10^6 cells per genotype) were intravenously inoculated into recipient mice carrying subcutaneous B16-gp33 tumors (1×10^6 cells injected 5 days before T-cell transfer). For in vitro activation, $CD8^+$ T lymphocytes were purified from the spleen and peripheral lymph nodes by negative selection. Naive $CD8^+$ T cells were activated with plate-bound anti-CD3 (2 μg/mL) and anti-CD28 (2 μg/mL) antibodies.

Tumor model and treatment

B16-F10 melanoma, MC38, and LLC-1 cells were cultured in complete DMEM (Gibco) supplemented with 10% FBS containing 100 units/mL penicillin-G, 100 μg/mL streptomycin (Gibco) and nonessential amino acids (Gibco). Tumor cells (1×10^6) were subcutaneously injected into the flanks of mice. TILs were isolated by dissociating tumor tissue in the presence of 1 mg/mL collagenase D for 1 h before centrifugation on a discontinuous Percoll gradient (Cytiva). Isolated cells were then used in various assays evaluating T-cell function. For the experimental metastasis assay, 1×10^6 B16-gp33 cells in a volume of 700 μL PBS were intravenously injected into the tail vein. After 18 days, the mice were sacrificed via cervical dislocation, and their lungs were removed and rinsed in phosphate-buffered saline. The number of B16-gp33 colonies on all five lobes of the lung was counted macroscopically. All mice used were of C57BL/6 background, both male and female, 8–12 weeks of age, and 25 (±5) g. Checkpoint blockade

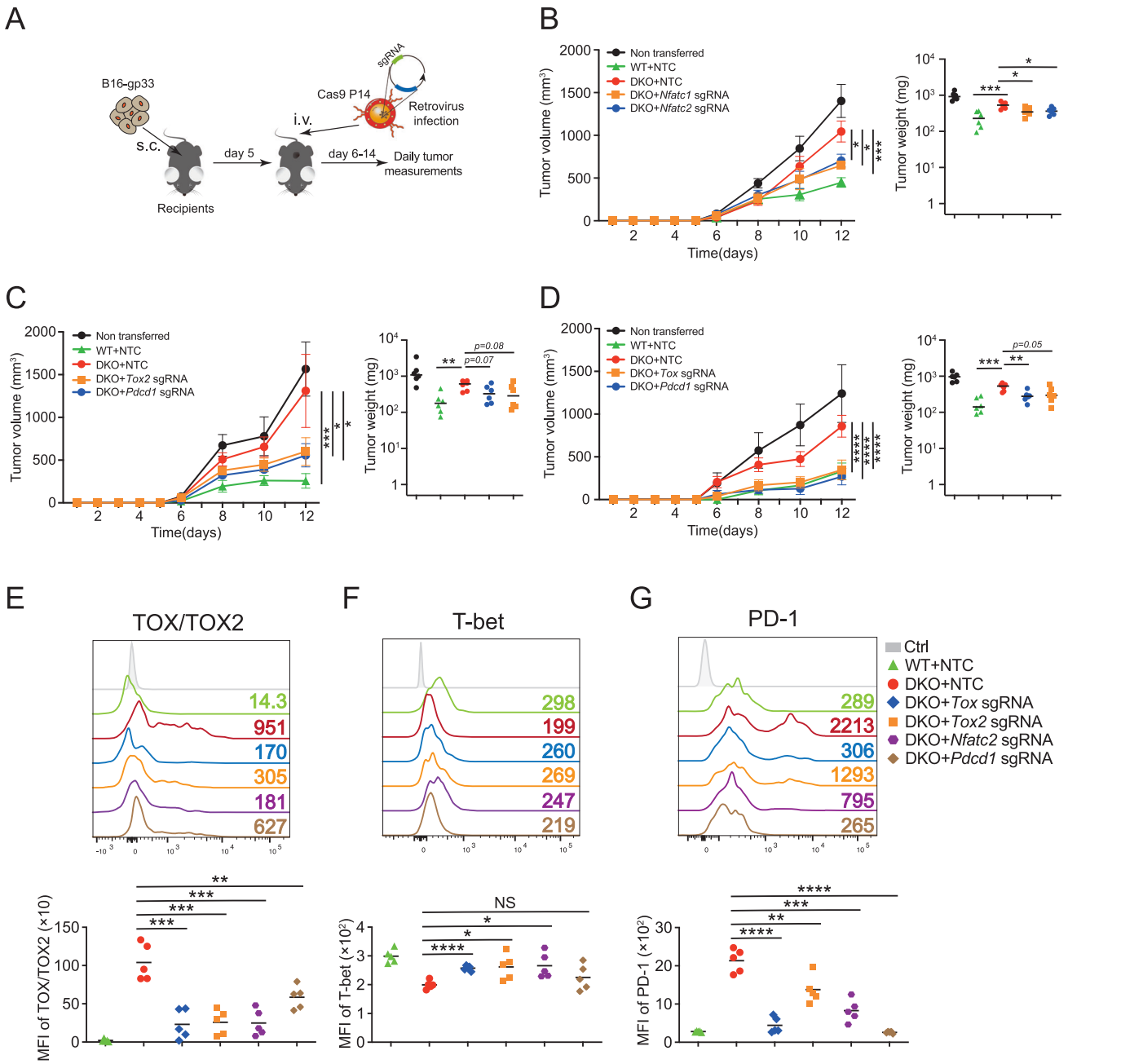

Fig. 7 *Nfatc1/Nfatc2* and *Tox/Tox2* deletion restores the anti-tumor function of DKO CD8$^+$ T cells. **A** Diagram of P14 transfer in a B16-gp33 melanoma model. P14 Cas9 cells were transduced with retroviruses encoding the indicated sgRNA and transferred into B16-gp33 tumor-bearing *Cd8*$^{-/-}$ hosts. **B-D** A total of 1×10^6 *Nfatc1* or *Nfatc2* (**B**), *Tox2* (**C**), *Tox* (**D**) or *Pdcd1* sgRNA-transduced Cas9 DKO P14 cells were transferred into *Cd8*$^{-/-}$ recipient mice 5 days after B16-gp33 inoculation. Tumor volume (left) and tumor weight of solid tumors isolated from mice on Day 14 (right). **E–G** A total of 1×10^6 NTC, *Tox*, *Tox2*, *Nfatc2*, or *Pdcd1* sgRNA-transduced Cas9 DKO P14 cells were transferred into recipient mice (CD45.1) that received B16-gp33 cells via tail vein injection ten days before. Flow cytometry analysis of TOX/TOX2 (**E**), T-bet (**F**), and PD-1 (**G**) expression among CD8$^+$CD45.2$^+$ Cas9$^+$ P14 cells in the lung (upper). Summary of MFI (lower). Each symbol represents an individual mouse. Small horizontal lines indicate the mean (±SD). Statistics in tumor volume (±SEM). *$P < 0.5$; **$P < 0.01$; ***$P < 0.001$; ****$P < 0.0001$. NS not significant. Data are representative of two independent experiments

therapy consisting of a combination of 200 mg of anti-PD-1 (RMP1-14, BioXCell) antibodies per dose or isotype control antibodies was administered on Days 6, 9, and 12 after tumor inoculation.

Antibodies and reagents

The following anti-mouse fluorochrome-conjugated antibodies were used for flow cytometric analysis: anti-TCR $V_{\alpha 2}$ (B20.1), anti-CD4 (GK1.5), anti-CD8a (53-6.7), anti-CD25 (PC61.5), anti-CD44 (IM7), anti-CD45.1 (A20), anti-CD45.2 (104), anti-CD62L (MEL-14), anti-CD69 (H1-2F3), anti-CD71 (R17217), anti-CD127 (A7R34), anti-KLRG1 (2F1), TIM3 (RMT3-23), LAG3 (eBioC9B7W), anti-IFNγ (XMG1.2), anti-TNFα (MP6-XT22), anti-granzyme B (NGZB), anti-Perforin (eBioOMAK-D), anti-TOX (TXRX10) and anti-Eomes (Dan11mag), all from eBioscience. Anti-PD-1 (29 F.1A12), anti-TIGIT (1G9), anti-T-bet (4B10), anti-Bcl2 (3F11), and anti-Ki67 (16A8) antibodies were purchased from BioLegend. Anti-Tox/Tox2 (E6G5O) was purchased from Cell Signaling. The following anti-mouse biotinylated antibodies were used to purify CD8$^+$ T cells: anti-B220 (RA3-6b2), anti-CD4 (GK1.5), anti-CD11b (M1-70), anti-CD11c (N418), anti-CD25 (PC61.5), anti-CD44 (IM7), anti-NK1.1 (PK136), anti-Ly-6G/Ly-6C (RB6-8C5), anti-F4/80 (BM8) and anti-TER119 (Ter119), all

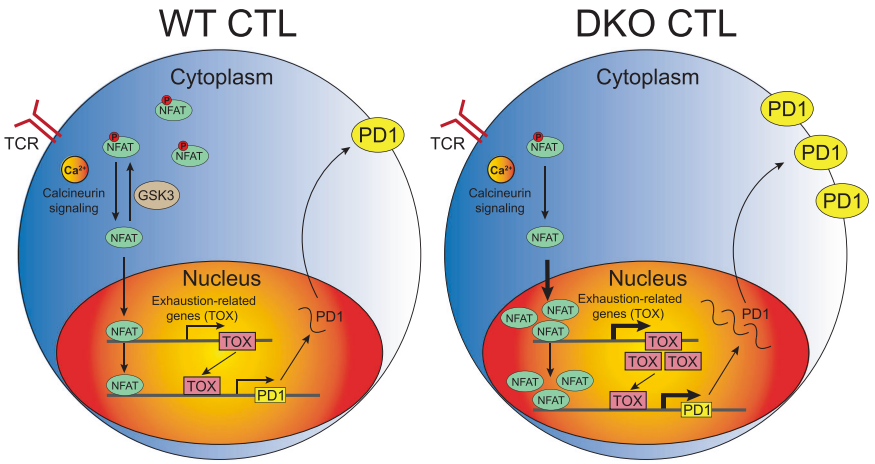

Fig. 8 GSK3 regulates T-cell exhaustion by suppressing activation of the NFAT-TOX axis: A model. Chronic TCR stimulation leads to sustained calcium influx, which promotes calcineurin-mediated dephosphorylation of NFAT. Dephosphorylated NFAT then translocates from the cytoplasm to the nucleus, where it transactivates the expression of exhaustion-related genes, including the transcription factor TOX/TOX2 and inhibitory receptor PD-1. TOX/TOX2 can also induce PD-1 expression. In contrast, GSK3-mediated NFAT phosphorylation results in the cytoplasmic retention of NFAT, thereby reducing NFAT-induced TOX/TOX2 and PD-1 expression. In the absence of GSK3, accumulated nuclear NFAT leads to the upregulation of TOX/TOX2 and PD-1 expression. Thus, GSK3 regulates the NFAT-activated T-cell exhaustion program by dampening the TCR-induced nuclear import of NFAT

from BioLegend. The following antibodies were used for Western blotting: anti-GSK3α/β (D75D3), anti-β-actin (13E5), anti-Tox/Tox2 (E6G5O) and anti-NFAT1 (D43B1) were from Cell Signaling Technology; anti-GAPDH (1E6D9), anti-LaminB1 (3C10G12), anti-β-Tubulin (1D4A4) and anti-Nfatc1 monoclonal antibodies (1E1B10) were from Proteintech; and anti-Bach2 (7A4) was from Abcam. PMA (phorbol 12-myristate 13-acetate) was purchased from Sigma. Ionomycin was purchased from Yeasen. Recombinant murine IL-2 and IL-7 were obtained from Novoprotein. The Fixation/Permeabilization Solution Kit and Annexin V/7-AAD Kit were purchased from BD Biosciences. The Foxp3 Transcription Factor Buffer Set was purchased from eBioscience. The EdU Flow Kit was purchased from Beyotime.

Flow cytometry

Single-cell suspensions were prepared from mouse spleen, lymph nodes (LNs), and tumors, and cells were passed through a 75 μm strainer, followed by lysis of erythrocytes with ACK (ammonium chloride-potassium). Tumors were excised, weighed, minced, and digested with collagenase for 1 h. Tumor-infiltrating leukocytes were isolated from tumors with Percoll. Fc block was performed by staining with anti-CD16/32 to avoid nonspecific binding. For cell surface marker staining, antibodies were combined in 30 μL FACS (fluorescence-activated cell sorting) buffer (PBS with 0.5% BSA and 0.05% NaN3), added to cells, and incubated at 4 °C for 30 min. For intracellular staining of transcription factors, after cell surface marker staining, cells were fixed and permeabilized for 30 min in Fix/Perm buffer (eBioscience). After washing with perm buffer, the cells were stained with antibodies for 1 h at room temperature. For intracellular staining of cytokines, cells were stimulated with PMA (50 ng/mL) and ionomycin (1 μg/mL) for 5 h before cytokine staining with the BD Fixation/Permeabilization Solution Kit. All flow cytometry data were acquired on a Fortessa or LSRFortessa X-20 (BD Biosciences) or a NovoCyte flow cytometer (ACEA Biosciences, Agilent) and analyzed with FlowJo software 10 (Treestar).

RNA sequencing and data analysis

Gsk3α$^{fl/fl}$*Gsk3β*$^{fl/fl}$ P14 (WT CD45.2) and *Gsk3α*$^{fl/fl}$*Gsk3β*$^{fl/fl}$ P14 *Gzmb* Cre (DKO, CD45.2) cells were intravenously injected (1×10^5 of each cell type) into B6 (CD45.1) hosts, followed by infection of the hosts 24 h later with LCMV-Arm. CD8$^+$ T cells were sorted from host mice at Day 5.5, and total RNA was isolated by Qiagen RNeasy Micro or Mini Kits following the manufacturer's instructions. RNA was quantified with a NanoDrop Nucleic Acid Analyzer. One microgram of RNA was used for RNA sequencing with a BGISEQ-500 instrument (BGI, Wuhan). Reads were aligned to the mm10 build of the *Mus musculus* genome with Hisat2. The alignments were passed to StringTie, which assembled and quantified the transcripts in each sample and generated gene count matrices. Differentially expressed genes were analyzed using the DESeq2 package. Genes were considered differentially expressed if they had an adjusted *P* value of 0.01 or less. Differentially expressed genes were analyzed with gene set enrichment analysis (GSEA) and the Mouse Genome Database (MGD) (www.informatics.jax.org) to find enriched biological processes and signaling pathways.

Retroviral transduction

Plat-E packaging cells were transfected with 2 μg of the retroviral vector along with PEI. At 48 and 72 h after transfection, retrovirus-containing supernatants were collected and stored at −80 °C. For retrovirus transduction, naive WT, and DKO P14 cells were isolated from spleen cell samples, followed by enrichment by CD8 negative selection. After 24 h of activation with anti-CD3 (2 μg/mL) and anti-CD28 (2 μg/mL) in the presence of recombinant murine IL-2 (20 ng/mL), P14 cells were transduced with retroviral supernatants containing polybrene (1 μg/mL) by centrifugation (1000 × g for 1 h at 37 °C).

Immunoblot analysis

For immunoblotting, whole cell extracts were lysed in lysis buffer [20 mM Tris-HCl (pH 7.5), 150 mM NaCl, 1% Triton X-100, 1 mM EDTA, and 1 mM EGTA] supplemented with Halt Protease and Phosphatase Inhibitor Cocktail. Lysates from equal numbers of cells were separated by 8% SDS PAGE and transferred to PVDF membranes (Merck Millipore), which were incubated with primary antibodies, followed by overnight incubation at 4 °C. After washing three times in TBST buffer, HRP-conjugated goat anti-rabbit or goat anti-mouse antibody was incubated with the membrane. After washing three times in TBST buffer, protein bands were visualized with Immobilon Western Chemiluminescent HRP Substrate (Merck Millipore). Images were acquired with an Amersham Imager 600 (GE Healthcare).

For the preparation of nuclear extracts, CD8$^+$ T cells were washed twice in PBS, and 1×10^7 cells were lysed in 0.15% NP-40 lysis buffer (10 mM HEPES, 10 mM KCl, 0.1 mM EDTA, 0.1 mM EGTA, and 0.15% NP-40) for 15 min on ice. The homogenates were centrifuged at full speed (12,000 g) for 3 min, and the supernatant was collected as cytoplasmic extracts. The nuclear pellet was washed three times with 0.15% NP-40 lysis buffer and resuspended in whole cell lysis buffer, followed by incubation on ice for 30 min.

Statistical analysis

All statistical analyses were performed with GraphPad Prism 9.0. Unpaired or paired Student's *t* tests and one-way ANOVA were used for data analysis. Statistical significance is displayed as NS not significant, $^*P < 0.05$; $^{**}P < 0.01$; $^{***}P < 0.001$ and $^{****}P < 0.0001$.

DATA AVAILABILITY

The data that support the findings of this study are available from the corresponding authors upon request.

REFERENCES

1. Chen DS, Mellman I. Oncology meets immunology: the cancer-immunity cycle. Immunity. 2013;39:1–10.
2. Denton AE, et al. Differentiation-dependent functional and epigenetic landscapes for cytokine genes in virus-specific CD8 + T cells. Proc Natl Acad Sci USA. 2011;108:15306–11.
3. Jenkins MR, et al. Cell cycle-related acquisition of cytotoxic mediators defines the progressive differentiation to effector status for virus-specific CD8 + T cells. J Immunol. 2008;181:3818–22.
4. Wherry EJ. T cell exhaustion. Nat Immunol. 2011;12:492–9.
5. Doering TA, et al. Network analysis reveals centrally connected genes and pathways involved in CD8 + T cell exhaustion versus memory. Immunity. 2012;37:1130–44.
6. Day CL, et al. PD-1 expression on HIV-specific T cells is associated with T-cell exhaustion and disease progression. Nature. 2006;443:350–4.
7. Wherry EJ, Kurachi M. Molecular and cellular insights into T cell exhaustion. Nat Rev Immunol. 2015;15:486–99.
8. Topalian SL, Drake CG, Pardoll DM. Immune checkpoint blockade: a common denominator approach to cancer therapy. Cancer Cell. 2015;27:450–61.
9. He R, et al. PD-1 and CTLA-4 inhibitors in combination vs. alone for the treatment of advanced melanoma: a systematic review and meta-analysis. Med (Baltim). 2022;101:e30561.
10. Nguyen LT, Ohashi PS. Clinical blockade of PD1 and LAG3–potential mechanisms of action. Nat Rev Immunol. 2015;15:45–56.
11. Araki K, Youngblood B, Ahmed R. Programmed cell death 1-directed immunotherapy for enhancing T-cell function. Cold Spring Harb Symp Quant Biol. 2013;78:239–47.
12. Martinez GJ, et al. The transcription factor NFAT promotes exhaustion of activated CD8(+) T cells. Immunity. 2015;42:265–78.
13. Man K, et al. Transcription factor IRF4 promotes CD8(+) T cell exhaustion and limits the development of memory-like T cells during chronic infection. Immunity. 2017;47:1129–41 e5.
14. Chen Y, et al. BATF regulates progenitor to cytolytic effector CD8(+) T cell transition during chronic viral infection. Nat Immunol. 2021;22:996–1007.
15. Seo H, et al. BATF and IRF4 cooperate to counter exhaustion in tumor-infiltrating CAR T cells. Nat Immunol. 2021;22:983–95.
16. Tsui C, et al. MYB orchestrates T cell exhaustion and response to checkpoint inhibition. Nature. 2022;609:354–60.
17. Muller MR, Rao A. NFAT, immunity and cancer: a transcription factor comes of age. Nat Rev Immunol. 2010;10:645–56.
18. Seo H, et al. TOX and TOX2 transcription factors cooperate with NR4A transcription factors to impose CD8(+) T cell exhaustion. Proc Natl Acad Sci USA. 2019;116:12410–12415.
19. Khan O, et al. TOX transcriptionally and epigenetically programs CD8(+) T cell exhaustion. Nature. 2019;571:211–18.
20. Scott AC, et al. TOX is a critical regulator of tumour-specific T cell differentiation. Nature. 2019;571:270–74.
21. Alfei F, et al. TOX reinforces the phenotype and longevity of exhausted T cells in chronic viral infection. Nature. 2019;571:265–69.
22. Yao C, et al. Single-cell RNA-seq reveals TOX as a key regulator of CD8(+) T cell persistence in chronic infection. Nat Immunol. 2019;20:890–901.
23. Fiol CJ, et al. Formation of protein kinase recognition sites by covalent modification of the substrate. Molecular mechanism for the synergistic action of casein kinase II and glycogen synthase kinase 3. J Biol Chem. 1987;262:14042–8.
24. Frame S, Cohen P, Biondi RM. A common phosphate binding site explains the unique substrate specificity of GSK3 and its inactivation by phosphorylation. Mol Cell. 2001;7:1321–7.
25. ter Haar E, et al. Structure of GSK3beta reveals a primed phosphorylation mechanism. Nat Struct Biol. 2001;8:593–6.
26. Ying QL, et al. The ground state of embryonic stem cell self-renewal. Nature. 2008;453:519–23.
27. Beals CR, et al. Nuclear export of NF-ATc enhanced by glycogen synthase kinase-3. Science. 1997;275:1930–4.
28. Beurel E, Michalek SM, Jope RS. Innate and adaptive immune responses regulated by glycogen synthase kinase-3 (GSK3). Trends Immunol. 2010;31:24–31.
29. Ohteki T, et al. Negative regulation of T cell proliferation and interleukin 2 production by the serine threonine kinase GSK-3. J Exp Med. 2000;192:99–104.
30. Taylor A, et al. Glycogen synthase kinase 3 inactivation drives T-bet-mediated downregulation of co-receptor PD-1 to enhance CD8(+) cytolytic T cell responses. Immunity. 2016;44:274–86.
31. Rudd CE, Chanthong K, Taylor A. Small molecule inhibition of GSK-3 specifically inhibits the transcription of inhibitory co-receptor LAG-3 for enhanced anti-tumor immunity. Cell Rep. 2020;30:2075–82 e4.
32. Pearce EL, et al. Control of effector CD8 + T cell function by the transcription factor Eomesodermin. Science. 2003;302:1041–3.
33. Intlekofer AM, et al. Effector and memory CD8 + T cell fate coupled by T-bet and eomesodermin. Nat Immunol. 2005;6:1236–44.
34. Liang C, et al. TOX as a potential target for immunotherapy in lymphocytic malignancies. Biomark Res. 2021;9:20.
35. Clevers H, Nusse R. Wnt/beta-catenin signaling and disease. Cell. 2012;149:1192–205.
36. Liu C, et al. Glycogen synthase kinase 3 drives thymocyte egress by suppressing beta-catenin activation of Akt. Sci Adv. 2021;7:eabg6262.
37. Crabtree GR, Olson EN. NFAT signaling: choreographing the social lives of cells. Cell. 2002;109:S67–79.
38. Kurachi M, et al. The transcription factor BATF operates as an essential differentiation checkpoint in early effector CD8 + T cells. Nat Immunol. 2014;15:373–83.
39. Chen L, et al. Structure of the DNA-binding domains from NFAT, Fos and Jun bound specifically to DNA. Nature. 1998;392:42–8.
40. Duran J, et al. GSK-3beta/NFAT signaling is involved in testosterone-induced cardiac myocyte hypertrophy. PLoS One. 2016;11:e0168255.
41. Kim MS, et al. Nerve growth factor (NGF) regulates activity of nuclear factor of activated T-cells (NFAT) in neurons via the phosphatidylinositol 3-kinase (PI3K)-Akt-glycogen synthase kinase 3beta (GSK3beta) pathway. J Biol Chem. 2014;289:31349–60.

ACKNOWLEDGEMENTS

We thank all members of the Liu Labs (Xiamen University) for the discussion and technical assistance. We thank Xiaohong Ma and Xiufeng Sun at the Xiamen University Flow Cytometry Core and Suqin Wu in the XMU Laboratory Animal Center for technical assistance.

AUTHOR CONTRIBUTIONS

YF conceived the study. YF, JW, and CL performed most of the mouse, cell, and molecular biology experiments. YF and JW performed RNA sequencing experiments. RT and KL analyzed the RNA sequencing data. YF, JW, and XG performed several of the molecular experiments. W-HL cosupervised the project. YF and W-HL wrote the manuscript with input from all authors.

FUNDING

This study was supported by the National Natural Science Foundation of China (31770953, 81830047, and 81961138008 to CX and 32070877 to W-HL), 1000 Young Talents Program of China (NX), and the Fundamental Research Funds for the Central Universities of China-Xiamen University (20720170064 to CX). The funders had no role in the study design, data collection, and analysis, decision to publish, or preparation of the manuscript.

COMPETING INTERESTS

The authors declare no competing interests.

ADDITIONAL INFORMATION

Supplementary information The online version contains supplementary material available at https://doi.org/10.1038/s41423-023-01075-0.

Correspondence and requests for materials should be addressed to Yubing Fu or Wen-Hsien Liu.